IEEE Access
Multidisciplinary | Rapid Review | Open Access Journal

Received February 1, 2020, accepted February 8, 2020, date of publication February 19, 2020, date of current version February 27, 2020.

Digital Object Identifier 10.1109/ACCESS.2020.2974414

Design and Experimental Evaluation of a 12 kW Large Synchronous Reluctance Motor and Control System for Elevator Traction

JING-CAN LI[1], MAO XIN[2], ZHEN-NAN FAN[3], AND REN LIU[1]

[1]State Key Laboratory of Power Transmission Equipment and System Security and New Technology, Chongqing University, Chongqing 400030, China
[2]Hzforward Electric Machinery Co., Ltd., Hangzhou 311305, China
[3]Key Laboratory of Fluid and Power Machinery, Ministry of Education, Xihua University, Chengdu 610039, China

Corresponding author: Zhen-Nan Fan (fanzhennan@126.com)

This work was supported in part by the National natural sciences fund youth fund of China, under Grant 51607146 and Grant 61703345, in part by the Key Scientific Research fund project of Xihua University, under Grant Z1520907 and Grant Z1520909, in part by the Key Research fund projects of Sichuan Provincial Education Department, under Grant 16ZA0155 and Grant 16ZB0159, in part by the Sichuan Science and Technology Program, under Grant 2018GZ0391, in part by the Chunhui Project Foundation of the Education Department of China, under Grant Z2016144, and in part by the Key Laboratory of Fluid and Power Machinery, Ministry of Education, Xihua university, Chengdu, China.

ABSTRACT Recently, a new type of motor, synchronous reluctance motor (SRM), has attracted wide attention from academia and industry because of its potential applications in fans, pumps, and elevator traction systems. Compared with traditional motors, these motors have lower eddy-current loss, less torque ripple, reduced noise, smaller moment of inertia, and faster dynamic response, and they provide a greater operating efficiency and safety and are simpler and easier to maintain. However, the ontology design and operation control of SRMs continue to be significant hurdles that must be overcome prior to practical implementation. In order to facilitate the practical application of SRMs in industry, at the invitation of an elevator company, we designed a large SRM for elevator traction. Herein, we describe the design of the proposed system and present a theoretical analysis of the system. Furthermore, we fabricate a real prototype and the corresponding control system and perform an experimental test under the rated operating conditions and 1.5× overload conditions in order to verify the SRM's performance. The results of the experimental testing were satisfactory and consistent with the theoretical calculations. At present, we have entered the stage of small-batch trial production and we expect to ultimately implement this novel design. Further, the approach to ontology design and operation control in this study can be used to inform the future development of novel SRMs.

INDEX TERMS Design, experimental evaluation, large synchronous reluctance motor, control system, elevator traction.

I. INTRODUCTION

Compared with traditional motors, synchronous reluctance motors mainly have the following advantages. First, the multi-laminated structure makes the hysteresis and eddy current loss on the rotor very small, and basically there is no rotor heating problem during synchronous operation, which improves the operating efficiency and safety of the motor. Second, the multi-laminated structure of the rotor makes the rotor surface smooth and the magneto-resistance changes are relatively continuous, which greatly reduces the torque ripple and noise of the motor during operation. Third, the rotor has no winding, the motor has small moment of inertia, fast dynamic response, and the motor is durable and easy to maintain. Fourth, high torque, strong overload capacity, easy to weak magnetic speed expansion. Fifth, the rotor speed depends on the frequency of the stator current, and the control system is simple and reliable. Therefore, in recent years, in the field of fan, pump and elevator traction, it has been widely concerned by academia and industry, and in the aspect of ontology design and operation control, some constructive achievements have been obtained [1]–[16]. However, because of its difficulty in ontology design and operation control, up to now, how to make this kind of motor better meet the

The associate editor coordinating the review of this manuscript and approving it for publication was Giambattista Gruosso.

TABLE 1. The basic performance parameters of the motor proposed by the elevator enterprise.

Parameter	Value
Rated load (N.m)	700
Rated output (kW)	12
Rated speed(rpm)	167
Percent torque ripple	≤6.5%
Maximun overload capacity	1.5 × rated load

TABLE 2. Main design parameters of motor stator.

Parameter	Value
The stator slot number	72
Outer diameter of the stator (mm)	510
Stator core length(mm)	180
Stacking factor of stator	0.95
Type of stator winding	Two-layer lap winding
Rotor pole number	6
Stacking factor of rotor	0.95
Silicon steel sheet type of stator	DW315_50
Silicon steel sheet type of rotor	DW315_50

actual industrial application requirements, such as greater power, better control reliability, higher operation safety, etc. in terms of ontology and control system design, still needs to be studied more widely and deeply.

At the invitation of an elevator company, we designed a large reluctance synchronous motor for the traction of elevators. In the subsequent work, we not only completed the design and analysis work, but also produced a real prototype and control system, and completed the test and verification work. Satisfactory results have been achieved. At present, we have entered the stage of small batch trial production.

And the basic design requirements of the synchronous reluctance motor proposed by the elevator enterprise are shown in TABLE 1.

II. THE DESIGN SCHEME OF SYNCHRONOUS RELUCTANCE MOTOR ONTOLOGY

A. THE MAIN PARAMETERS OF SRM ONTOLOGY

After testing, analyzing, and comparing a series of alternative designs for the SRM body, the main structure and material parameters were determined, as shown in TABLE 2. The structure of the motor is shown in Fig. 1.

B. THE MATHEMATICAL MODEL OF THE SRM

In **SRM** motor, the high permeability path is referred to as the direct-axis path, while the low permeability path is referred to as the quadrature-axis path, as shown in Fig. 1.

It is observed that higher flux linkage along d-axis, while the q-axis flux linkage is limited by the rotor flux barriers.

The electrical equations in a rotating rotor d-q reference frame, describing the dynamic behavior of the SRM's stator voltage, neglecting saturation and skin-effect, can be expressed as:

$$\begin{aligned} u_{sd} &= \frac{d\psi_d}{dt} - \omega_s \cdot \psi_q + R \cdot i_{sd} \\ u_{sq} &= \frac{d\psi_q}{dt} + \omega_s \cdot \psi_d + R \cdot i_{sq} \end{aligned} \tag{1}$$

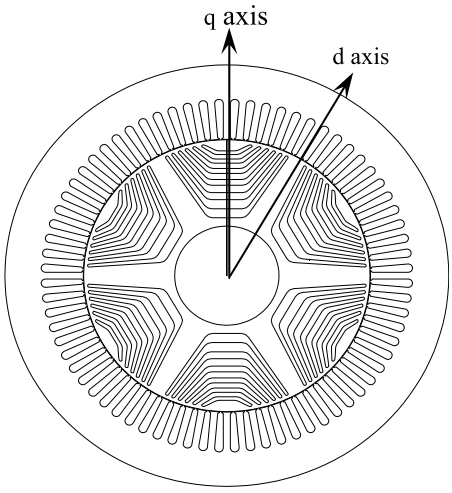

FIGURE 1. 2D structure of the proposed SRM.

The flux linkages can be expressed as:

$$\begin{aligned} \psi_d &= L_d \cdot i_{sd} \\ \psi_q &= L_q \cdot i_{sq} \end{aligned} \tag{2}$$

The average torque can be calculated as:

$$T_{em} = \frac{3}{2} p \cdot (L_d - L_q) \cdot i_{sd} \cdot i_{sq} \tag{3}$$

where

i_{sd}, i_{sq}	d and q-axis components of armature current;
u_{sd}, u_{sq}	d and q-axis components of terminal voltage;
R	armature resistance;
Ψ_d, Ψ_q	d and q-axis stator flux linkage
L_d, L_q	the d- and q-axes of armature self inductances;
p	number of pole pairs;
ω_s	the Rotor electrical speed;
T_{em}	electromagnetic torque.

III. THE DESIGN SCHEME OF SYNCHRONOUS RELUCTANCE MOTOR CONTORL SYSTEM

A. THE OVERALL TECHNICAL SCHEME OF CONTROL SYSTEM

According to the technical index and operational requirements for industrial elevator motors, the following general technical solutions were adopted. The direct current (DC) bus voltage was regulated by filtering after uncontrollable rectification of the three-phase alternating current (AC) power frequency. A three-phase fully controlled pulse width modulation (PWM) converter was implemented to drive the SRM. A digital signal processor (DSP) chip was used to control the PWM converter to realize drive control of the SRM. The SRM can operates in either rotational-speed-control or torque-control mode. When braking, the feedback energy is consumed by controlling the bleeder circuit.

The converter on the motor side adopts a three-phase inverter–rectifier bridge composed of an intelligent power module (IPM). During operation, the input voltage and

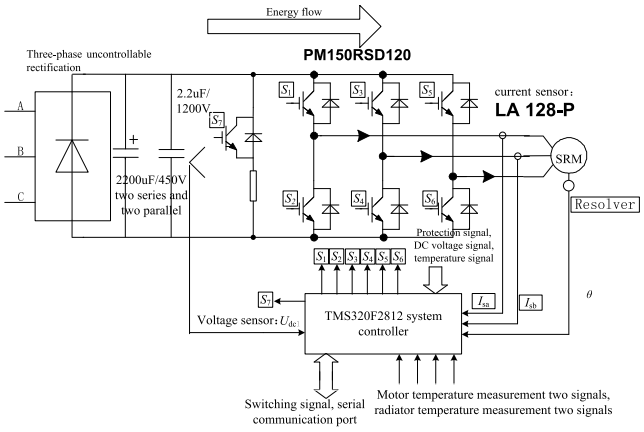

FIGURE 2. The schematic diagram of main power circuit.

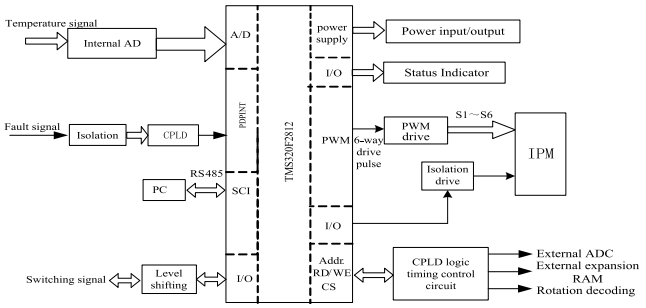

FIGURE 3. Schematic diagram of the main control circuit.

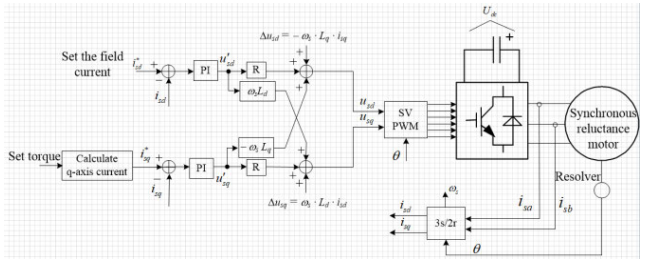

FIGURE 4. Principle block diagram of motor control.

current are controlled by PWM to achieve the desired high torque output.

In order to acquire information regarding the motor's rotor position, a sensor-based scheme using a resolver as a position sensor was adopted. While a sensorless method may be more innovative, it requires highly accurate motor control parameters; however, it would be difficult to accurately obtain the required motor performance parameters and rotor position information in a timely manner, considering that sometimes the load and current of the elevator motor change rapidly and violently (e.g., during the elevator's start-up stage). Thus, the sensorless scheme is undoubtedly extremely unfavorable for the safety of the elevator and its passengers.Therefore, in order to ensure the reliability, accuracy, and safety of the control system and the elevator, a sensor-based method was ultimately adopted,and a resolver was implemented as the motor's rotor position sensor.On this basis,by controlling the magnetic field and torque current of the motor, the operating requirements of the motor at each operating point can be satisfied.

The main controller of the motor is a 32-bit fixed-point DSP, TMS320F2812, produced by Texas Instruments (TI) (Dallas, TX, USA). This processor was used to run the motor start-up; control the speed and torque of the motor; and provide overvoltage, overcurrent, and overheating protection for the motor and other main components of the system.And also provide the data communication interface, analog quantity interface and relevant switching quantity interface connected with the upper system.

B. THE MAIN POWER LOOP DESIGN

As shown in Fig. 2, the main power loop for synchronous reluctance consists of three-phase uncontrollable rectification; large capacitance filtering; an IPM; sampling of the current, voltage, temperature, speed, and position signals; and system controler.

The basic working principle of the main power circuit is as follows: Under normal operating conditions, the power frequency three-phase AC (line voltage: 380V, 50Hz) is rectified into a large ripple DC after passing through a three-phase uncontrolled rectifier bridge.And through 2,200 μF/450V capacitors (connected two in series and two in parallel) and a 2.2μF/1,200V high-frequency capacitor, the DC-side voltage becomes relatively stable and the ripple is greatly improved. After the DC-side voltage passes through the IPM, it is directly applied to the three-phase stator winding of the SRM.

The TMS320F2812 system controller samples the DC-side bus voltage, stator current, and position and speed signals in real time and then sends out the six-channel PWM signal (usually space vector PWM [SVPWM]) after processing to drive the IPM,so as to realize the closed-loop control of synchronous reluctance motor.

When the motor needs to stop, the energy is fed back to the DC-side and the voltage sensor monitors the higher DC-side voltage, which changes the state of S7; the bleeder resistance will be added to the DC-side. At this time, the energy returned via the feedback loop will be on the bleeder resistance, and it will not cause the DC-side voltage to be too high and burn out the device.

C. THE HARDWARE CIRCUIT DESIGN

As shown in Fig.3, the main control loop of the synchronous reluctance motor includes the DSP minimum system, power supply circuit, CPLD logic timing control circuit, internal ADC, external ADC, resolver decoding circuit, SCI communication circuit, SPI circuit, IO, And PWM circuit.

The main control chip of this design scheme is TI's TMS320F2812. Its minimum system includes chip power supply (3.3V, 1.9V), 30M passive crystal oscillator, 14-pin JTAG port, plus a small amount of resistors and capacitors, jumpers.

The JTAG port is generally used to communicate with the DSP in the process of program debugging. When the debugging program is more mature, the program can be burned

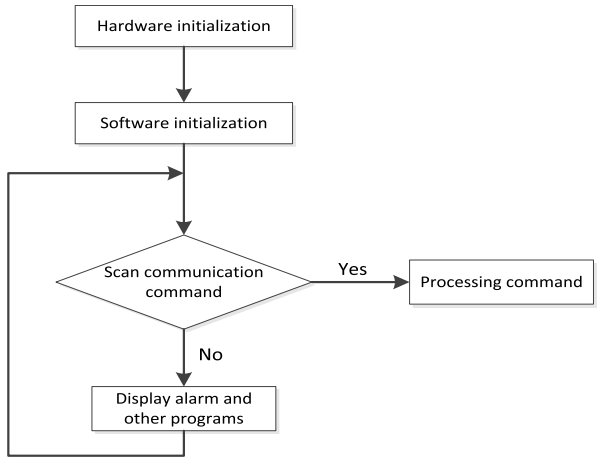

FIGURE 5. Main program control block diagram.

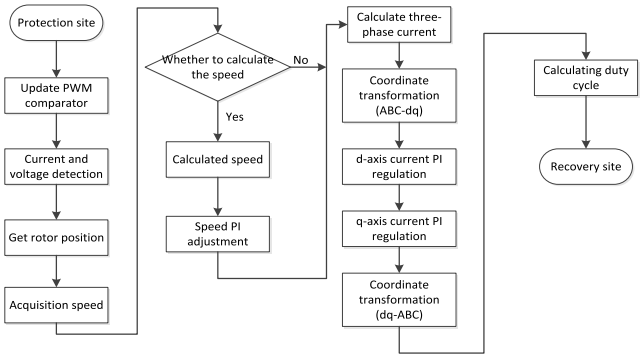

FIGURE 6. CPU timer 0 interrupt service routine.

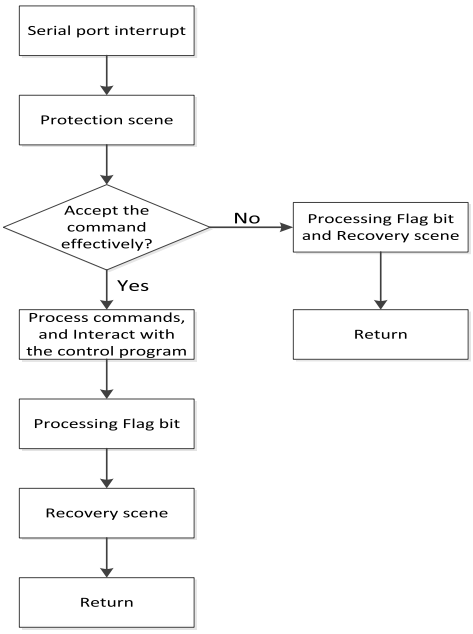

FIGURE 7. Serial port interrupt service routine.

to the on-chip FLASH without making any major changes. Further, the SCI can be used directly for communication between the DSP and the PC.

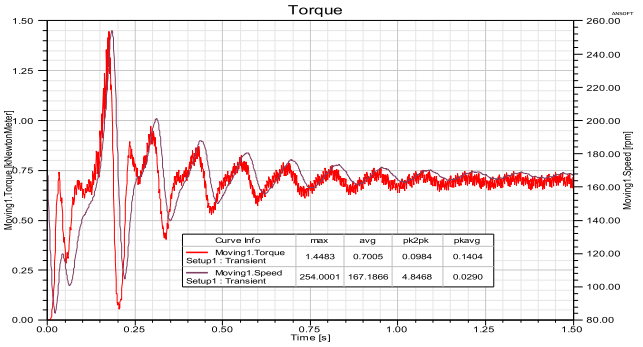

(a)Torque

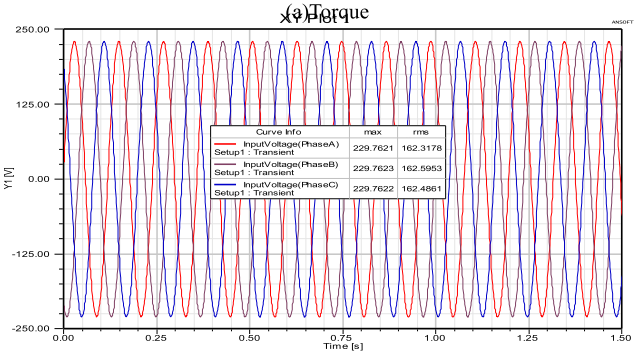

(b)Phase voltage

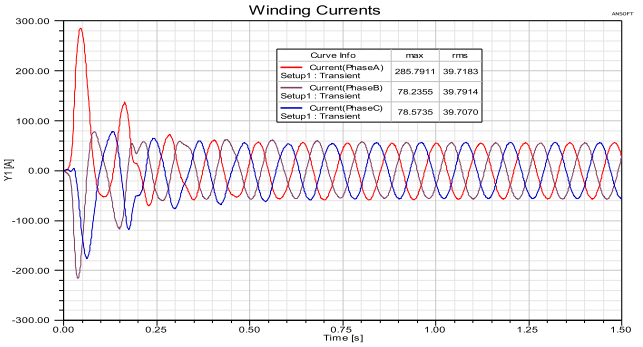

(c)Phase current

FIGURE 8. Torque, phase voltage, and phase current under the rated load conditions (167rpm, load: 700N·m).

D. THE CONTROL SOFTWARE DESIGN

Fig.4 shows a principle block diagram of the operation control of the SRM.The SRM adopts a vector-control mode, and the current loop can be used to control the starter motor to achieve the starting speed. When the motor needs to be started, the q-axis starting current is calculated according to the set starting torque. The current component property is the drag current, and the appropriate field magnet current ($i*_{sd}$) can be set to generate the starting torque. Detecting the current input into the three-phase winding of the motor and using the coordinate transformation of three phases to two phases, the currents on the d- and q-axes (i_{sd} and i_{sq}) are obtained. These values are compared with the given values, and the d- and q-axis voltage reference values (u_d and u_q) are calculated by the respective PI regulators using the voltage equations associated with the d- and q-axes and the current loop cross-coupling term. Finally, by applying SVPWM, the converted PWM drive pulse is inputted into the

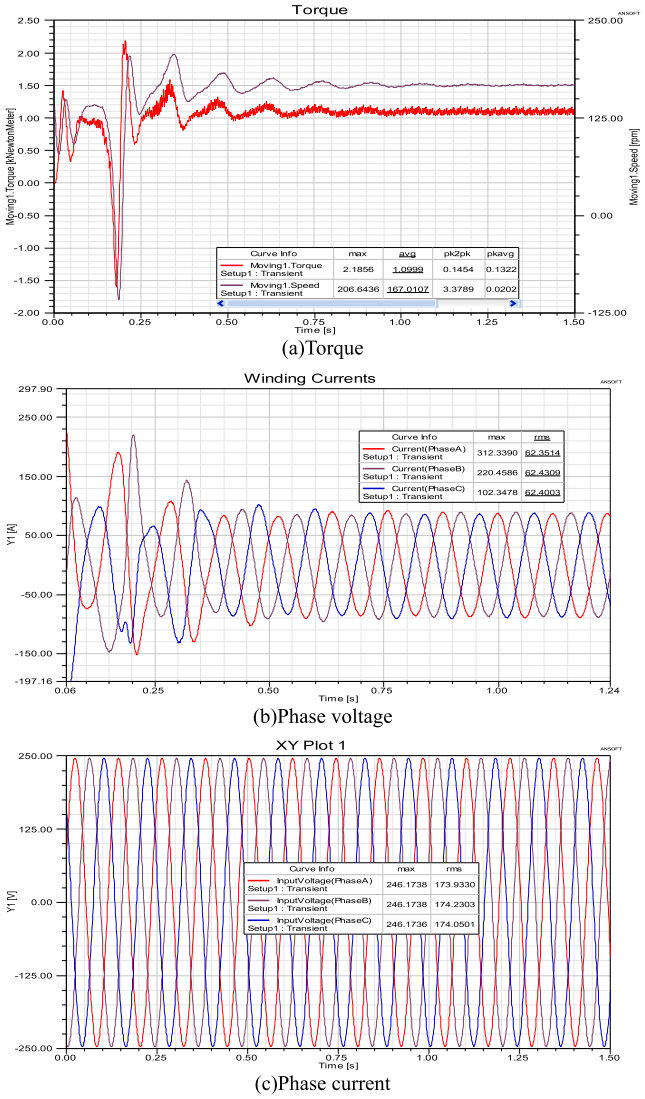

FIGURE 9. Torque, phase voltage, and phase current under 1.5× rated load conditions (167rpm, load: 1,100N·m).

three-phase PWM converter to generate a three-phase sinusoidal current through the stator windings of the motor to achieve control of the SRM.

A block diagram of the main controller is shown in Fig. 5. First, the clock of the DSP and the state of the peripheral are initialized. The clock frequency of the system is 150MHz, and each single instruction cycle is 6.67ns. The software of the interrupt, event manager, SPI, and SCI, among others, is initialized and enters the main control program, which is nested within the timer-0 interrupt with a control period of 100μs. During each control cycle, when the main control-program is executed, the CPU continuously scans to check whether there is a command issued by the host computer; if so, the program is executed; if not, the scanning continues until the next control cycle.

As shown in Fig. 6, in the main control program, the scene is first protected and then the comparison value in the PWM comparator is updated. Then, the ADC is started; the current

TABLE 3. Main design parameters of motor rotor.

	Rated load	1.5 times rated load
Rotating speed（rpm）	167	167
Line voltage rms（V）	281.62	301.77
Phase voltage rms（V）	162.6	39.8
Current rms（A）	39.8	62.5
Current density（A/mm^2）	3.7537	5.8947
Output torque（Nm）	700	1100
Output Power（kW）	12.241	19.235
Percent torque ripple	6%	6.12%
Torque-to-current ratio	17.58	17.60

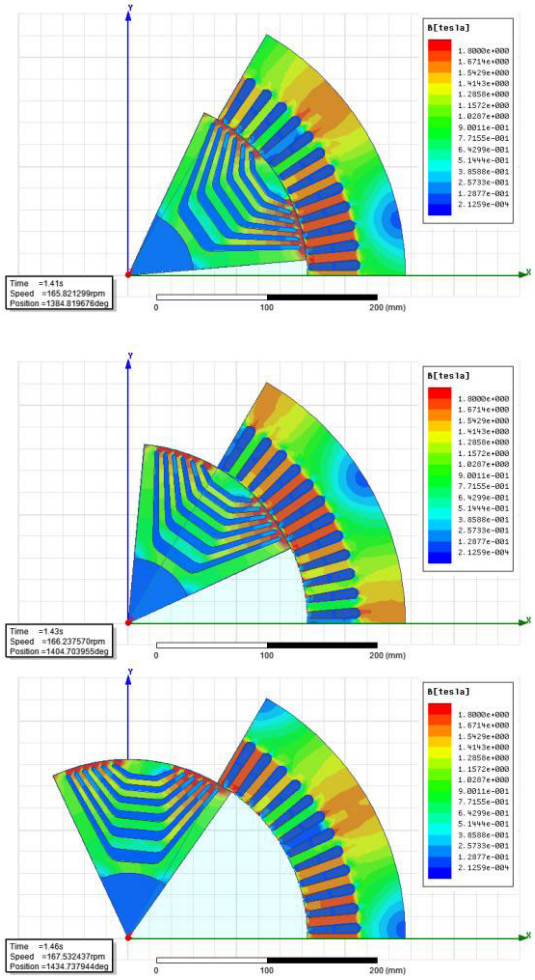

FIGURE 10. The magnetic field distribution in the motor at different times (rated operation).

signal, DC-side voltage, and rotor position are sampled; and the speed reference is obtained to determine whether the speed should be calculated (as it generally takes 10 control cycles to calculate the rotational speed in the program). If the speed is calculated, the PI regulator is added to adjust the speed; if not, the three-phase current is calculated, the current d- and q-axis currents are calculated by coordinate transformation, and the d- and q-axis currents are adjusted by the PI regulator. Finally, the stator voltage is calculated once again by coordinate transformation, the duty cycle is calculated, and the scene is restored.

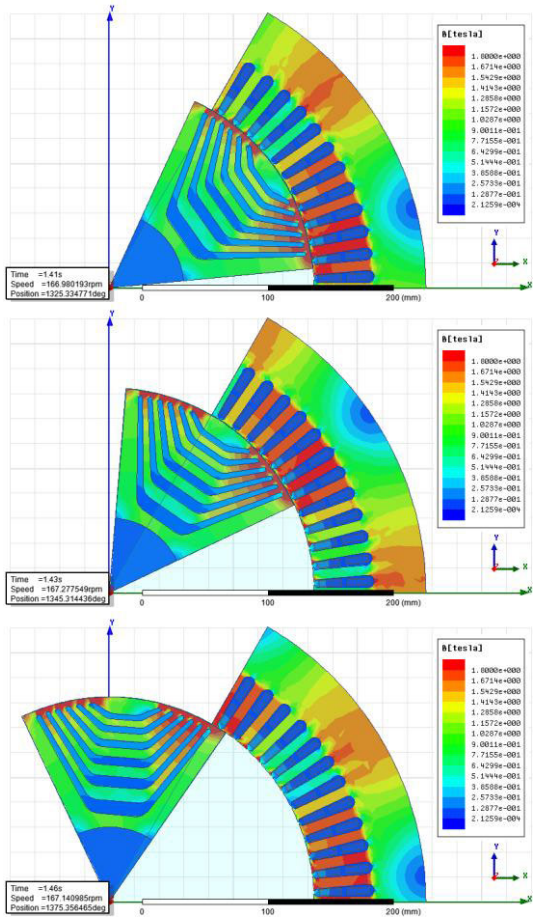

FIGURE 11. The magnetic field distribution in the motor at different times (1.5 times overload operation).

As shown in Fig. 7, in each control cycle, the CPU continuously scans the serial port interrupt flag bit after executing the main control program. If the serial port interrupt flag is set, the response is interrupted, the scene is protected, and it is judged whether the command is valid according to the communication protocol. If it is valid, the program will be executed, then the flag bit will be cleared, and the system will return to its previous state; if it was deemed to be invalid, the flag bit will be cleared and the system will return to its previous state.

IV. ELECTROMAGNETIC ANALYSIS RESULTS AND DISCUSSIONS

In view of the proposed SRM design scheme, the performance was evaluated under the rated operation conditions and 1.5× overload conditions in terms of the voltage, current, and torque using the time-stepping finite element method. The results are summarized in Figs. 8 and 9 and TABLE 3.

The electromagnetic analysis results indicated that, in theory, the performance of the motor (e.g., speed, output electromagnetic torque, output power, and percent torque ripple) meets the design requirements under its rated operating conditions and 1.5× overload.

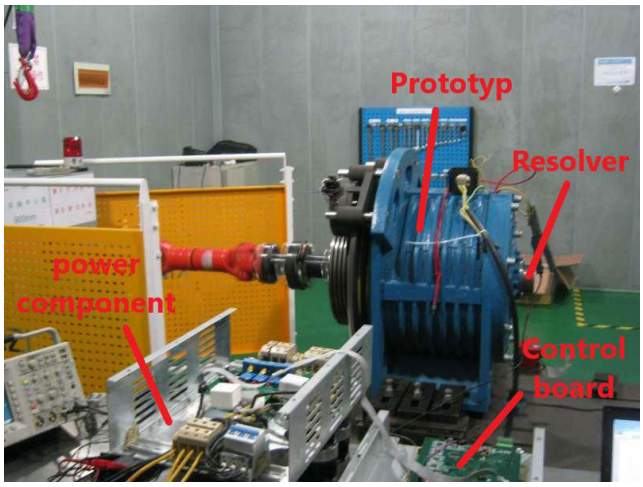

FIGURE 12. The prototype test scenarios.

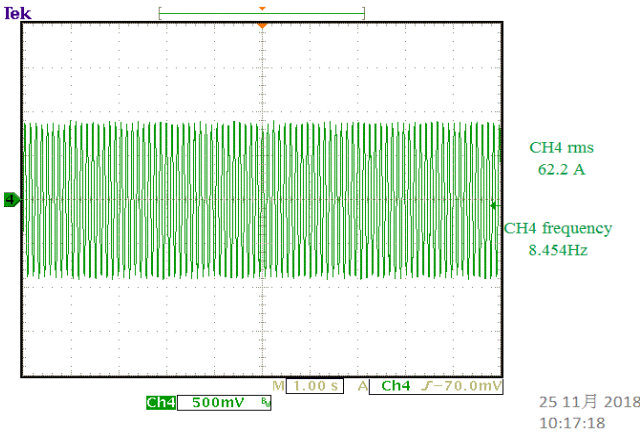

FIGURE 13. Stator current test waveform during 1.5× overload operation(time:10:17/25/11/2018).

Further, no serious magnetic saturation occurred in the internal magnetic field distribution of the motor under either set of conditions, as shown in Figs. 10 and 11. Therefore, it can be considered that, theoretically, the magnetic circuit design of the motor is reasonable and offers good material utilization.

V. PROTOTYPE TEST RESULRS AND DISCUSSIONS

Next, a prototype and a control system were fabricated according to the design scheme. A real operation test was carried out under the rated load operating conditions and 1.5× overload conditions on November 25, 2018. The test scenarios is shown in Fig. 12.

A. THE 1.5 × OVER LOAD OPERATING TES

At the same time,from the envelope of the current waveform,it can be seen that the operation of the motor is relatively stable, In the 1.5× overload operation experiment, in order to protect the motor, 1.47× rated load was applied (i.e., the load torque was 1030 N·m). The motor successfully dragged this load and ran steadily for more than 3 min.

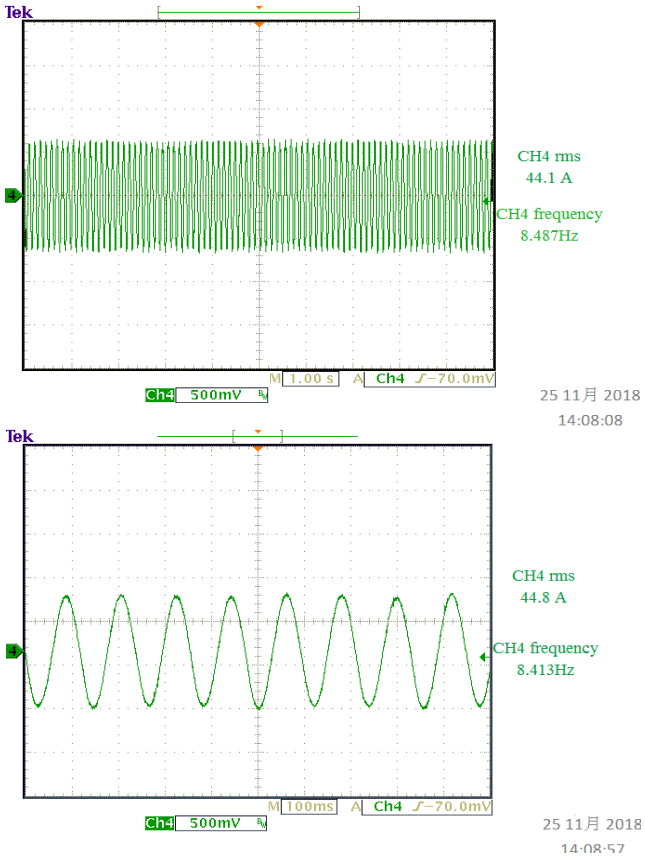

FIGURE 14. Stator current test waveforms under the rated load conditions(time:14:08/25/11/2018).

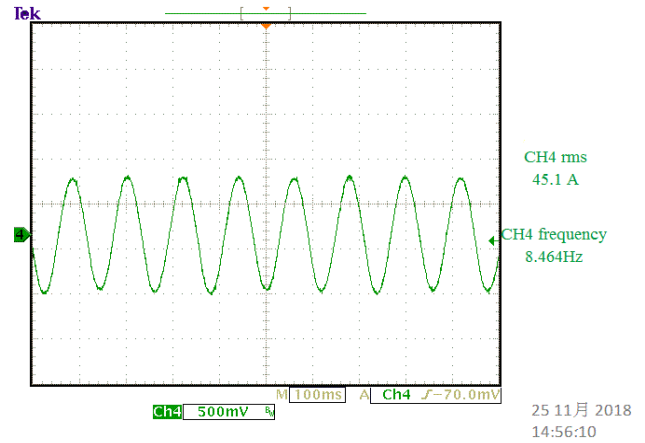

FIGURE 15. Stator current test waveforms under the rated load conditions(time:14:56/25/11/2018).

Fig.13 shows the stator current waveform during the overload test. The effective current was $I = 62.2$ A, the speed was $n = 169.08$ r/min, the torque was $T = 1030$ N·m, and the torque-to-current ratio was16.56; these values were very close to the calculated values of 62.5, 167, 1100, and 17.58, respectively (TABLE 3).

Furthermore, from the envelope of the current waveform, it can be concluded that the operation of the motor was relatively stable under these conditions.

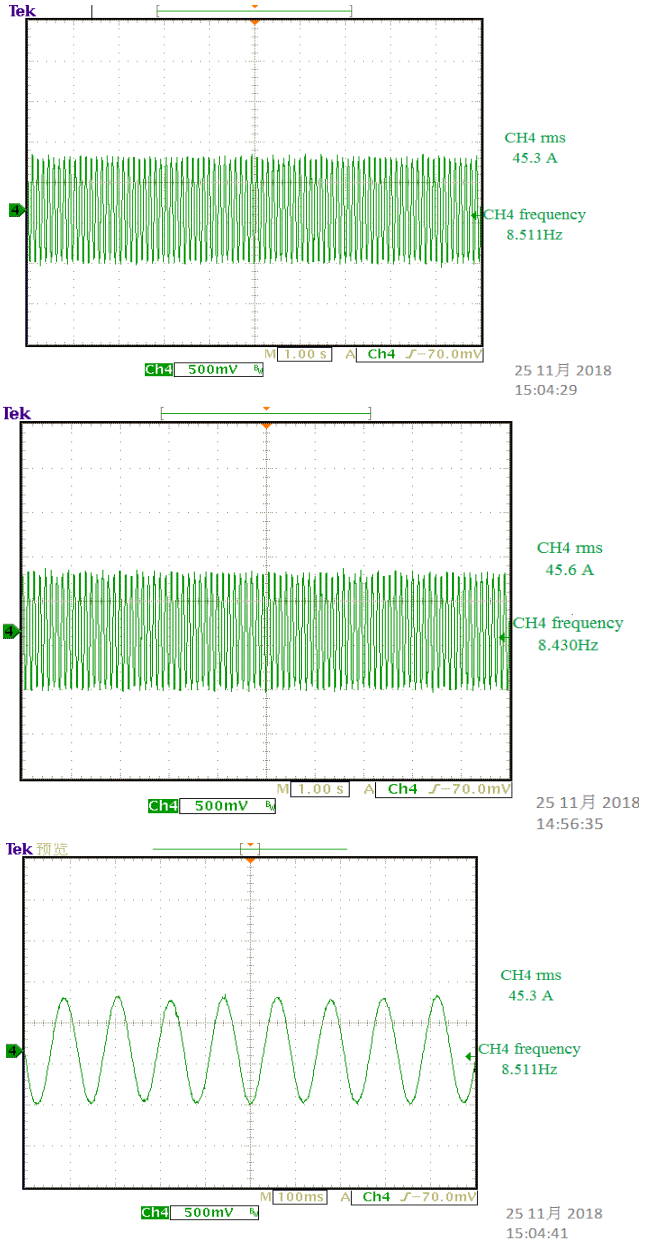

FIGURE 16. Stator current test waveforms under the rated load conditions(time:15:04/25/11/2018).

B. THE RATED LOAD OPERATING TEST

Figs.14 to 16 shows records of stator current waveforms during the operation test under the rated conditions; in this case, the motor had been running stably for 1h. In the operation experiment under the rated conditions, after entering the stable rated operation state, the motor's torque fluctuated in the range of 696–701N.m; however, it can be considered that the torque was stable around T = 700N.m. At the same time, the speed was stable around 168–169r/min. Further, the current was stable at I = 44.3A, and the torque-to-current ratio was approximately 15.8. These values were very close to the calculated values of 39.8and 17.58, respectively (TABLE 3).

Over the time course of the test, the temperatures of the stator's core and surface increased. It can be seen from Fig. 16 that the current was I = 45.3A; this is because the stator's resistance increases with the rise in temperature. As shown in Figs. 14–16, the sinusoidality of the current was very good under the rated operating conditions.

Further, in the case of Figs. 14–16, the envelope of the current was small. Owing to the use of PWM and limited carrier frequency, the program can be optimized later to make the envelope smaller.

From the above experimental results and analysis with the prototype, it can be seen that the 12kW SRM proposed herein exhibits an acceptable performance that is highly consistent with the theoretical calculations. Therefore, it can be considered that the design is suitable for further testing and, ultimately, implementation for elevator traction systems.

VI. CONCLUSION

In this paper, at the invitation of an elevator company, we designed a12kW large SRM for elevator traction. Here, we reported the design and analysis work and conducted testing and validation on a real prototype and control system. Satisfactory results were obtained experimentally, and these results were consistent with the theoretical calculations. Therefore, we cautiously consider that the design and trial production of this prototype (12kW SRM) and its control system are successful, which have certain applicable value in engineering. At present, we are in a small-batch trial production stage for the further test and improvement of this kind of motor.

However, at the same time, we realize that, in recent years, some excellent researchers have made great progress on the sensorless control technology of motor, emerging fruitful achievements [17]–[22]. It provides valuable references to improve the control level of SRM,this is the research direction we will pay attention to in the future. At the same time, we will focus on how to combine the optimization algorithm to further improve the SRM design. We plan to conduct in-depth study on these points with new papers.

REFERENCES

[1] S. E. Lyshevski, A. El-Antably, and A. M. El-Sharkawy, "Synchronous reluctance motors:Nonlinear analysis and control," in *Proc. Amer. Control Conf.*, vol. 2, 2000, pp. 1108–1112.

[2] N. Aros, V. Mora, and C. Alarcon, "Model predictive control for synchronous reluctance motor drive," in *Proc. Conf. Electr., Electron. Eng., Inf. Commun. Technol. (CHILECON)*, Oct. 2017, pp. 1–6.

[3] A. V. Zakharov, S. I. Malafeev, and A. L. Dudulin, "Synchronous reluctance motor: Design and experimental research," in *Proc. Int. Conf. Elect. Power Drive Syst. (ICEPDS)*, Oct. 2018, pp. 1–4.

[4] H.-S. Hong, H.-C. Liu, S.-Y. Cho, J. Lee, and C.-S. Jin, "Design of high-end synchronous reluctance motor using 3-D printing technology," *IEEE Trans. Magn.*, vol. 53, no. 6, pp. 1–5, Jun. 2017.

[5] B. Poudel, E. Amiri, and P. Rastgoufard, "Design and analysis of line start synchronous reluctance motor with dual saliency," in *Proc. IEEE Transp. Electrific. Conf. Expo. (ITEC)*, Jun. 2018, pp. 385–388.

[6] D.-Q. Nguyen, L. Loron, and K. Dakhouche, "High-speed sensorless control of a synchronous reluctance motor based on an Extended Kalman Filter," in *Proc. 17th Eur. Conf. Power Electron. Appl. (EPE)*, Sep. 2015, pp. 1–10.

[7] M. Popescu, J. E. Goss, D. A. Staton, Y. Wang, and D. M. Ionel, "On the feasibility of integer and fractional number of slots per pole distributed winding designs for synchronous reluctance motors," in *Proc. IEEE Energy Convers. Congr. Expo. (ECCE)*, Sep. 2014, pp. 5144–5151.

[8] I.-H. Lin, M.-F. Hsieh, H.-F. Kuo, and M.-C. Tsai, "Improved accuracy for performance evaluation of synchronous reluctance motor," *IEEE Trans. Magn.*, vol. 51, no. 11, pp. 1–4, Nov. 2015.

[9] Y. Wang, D. Ionel, D. G. Dorrell, and S. Stretz, "Establishing the power factor limitations for synchronous reluctance machines," *IEEE Trans. Magn.*, vol. 51, no. 11, pp. 1–4, Nov. 2015.

[10] C. Spargo, B. Mecrow, and J. Widmer, "Synchronous reluctance motors with toroidal windings," in *Proc. IEEE Energy Convers. Congr. Expo. (ECCE)*, Sep. 2014, pp. 1374–1378.

[11] K. Malekian, M. R. Sharif, and J. Milimonfared, "An optimal current vector control for synchronous reluctance motors incorporating field weakening," in *Proc. IEEE Int. Workshop Adv. Motion Control*, May 2008, pp. 393–398.

[12] M. Mirzaei and S. E. Abdollahi, "Design optimization of reluctance-synchronous linear machines for electromagnetic aircraft launch system," *IEEE Trans. Magn.*, vol. 45, no. 1, pp. 389–395, Jan. 2009.

[13] H.-S. Kim and J.-H. Lee, "The sensorless vector control characteristics analysis of synchronous reluctance motor using a coupled FEM & Preisach model," in *Proc. Int. Conf. Elect. Mach. Syst. (ICEMS)*, Dec. 2007, pp. 1210–1215.

[14] A. Boglietti, A. Cavagnino, M. Pastorelli, D. Staton, and A. Vagati, "Thermal analysis of induction and synchronous reluctance motors," *IEEE Trans. Ind. Appl.*, vol. 42, no. 3, pp. 675–680, May 2006.

[15] M. Hinkkanen, H. A. A. Awan, Z. Qu, T. Tuovinen, and F. Briz, "Current control for synchronous motor drives direct discrete-time pole-placement design," *IEEE Trans. Ind. Appl.*, vol. 52, no. 2, pp. 1530–1541, Oct. 2015.

[16] P. Li, W. Ding, and G. Liu, "Sensitivity analysis and design of a high performance permanent-magnet-assisted synchronous reluctance motor for EV application," in *Proc. IEEE Transp. Electrific. Conf. Expo. (ITEC)*, Jun. 2018. pp. 406–411.

[17] X. Sun, Z. Shi, G. Lei, Y. Guo, and J. Zhu, "Analysis and design optimization of a permanent magnet synchronous motor for a campus patrol electric vehicle," *IEEE Trans. Veh. Technol.*, vol. 68, no. 11, pp. 10535–10544, Nov. 2019, doi: 10.1109/TVT.2019.2939794.

[18] X. Sun, K. Diao, G. Lei, Y. Guo, and J. Zhu, "Study on segmented-rotor switched reluctance motors with different rotor pole numbers for BSG system of hybrid electric vehicles," *IEEE Trans. Veh. Technol.*, vol. 68, no. 6, pp. 5537–5547, Jun. 2019.

[19] Z. Shi, X. Sun, Y. Cai, Z. Yang, G. Lei, Y. Guo, and J. Zhu, "Torque analysis and dynamic performance improvement of a PMSM for EVs by skew angle optimization," *IEEE Trans. Appl. Supercond.*, vol. 29, no. 2, pp. 1–5, Mar. 2019, doi: 10.1109/TASC.2018.2882419.

[20] X. Sun, Y. Shen, S. Wang, G. Lei, Z. Yang, and S. Han, "Core losses analysis of a novel 16/10 segmented rotor switched reluctance BSG motor for HEVs using nonlinear lumped parameter equivalent circuit model," *IEEE/ASME Trans. Mechatronics*, vol. 23, no. 2, pp. 747–757, Apr. 2018.

[21] X. Sun, K. Diao, Z. Yang, G. Lei, Y. Guo, and J. Zhu, "Direct torque control based on a fast modeling method for a segmented-rotor switched reluctance motor in HEV application," *IEEE Trans. Emerg. Sel. Topics Power Electron.*, to be published, doi: 10.1109/JESTPE.2019.2950085.

[22] X. Sun, J. Cao, G. Lei, Y. Guo, and J. Zhu, "Speed sensorless control for permanent magnet synchronous motors based on finite position set," *IEEE Trans. Ind. Electron.*, to be published, doi: 10.1109/TIE.2019.2947875.

JING-CAN LI was born in Yichang, China, in 1977. He received the Ph.D. degree in electrical engineering from Chongqing University, Chongqing, China, in 2011. He is currently a Lecturer with Chongqing University. His research interests include magnetic and thermal field calculation of generators, electrical machinery, motor drives, and the control of electrical machines.

MAO XIN was born in Jiaocheng, China, in 1982. He received the M.S. degree in electrical engineering from Chongqing University, Chongqing, China, in 2005. He is currently an Electrical Engineer with Hzforward Electric Machinery Co., Ltd., Hangzhou, China. His research interests include magnetic and thermal field calculation of generators, electrical machinery, motor drives, and the control of electrical machines.

ZHEN-NAN FAN was born in Longchang, China, in 1981. He received the Ph.D. degree in electrical engineering from Chongqing University, Chongqing, China, in 2013. He is currently an Associate Professor with Xihua University. His research interests include magnetic and thermal field calculation of generators, electrical machinery, and motor drives.

REN LIU was born in Dazhou, China, in 1979. He received the Ph.D. degree in electrical engineering from Chongqing University, Chongqing, China, in 2008. He is currently a Lecturer with Chongqing University. His research interests include magnetic and thermal field calculation of generators, electrical machinery, motor drives, and the control of electrical machines.